Eur. J. Mech. B - Fluids 20 (2001) 145–153

S0997-7546(00)01100-6/FLA

Partial roll-up of a viscoelastic Kármán street

Olivier Cadot

Laboratoire de Mécanique, Université du Havre, 25 rue Philippe Lebon, 76058 Le Havre, France

(Received 18 February 2000; revised 9 June 2000; accepted 15 June 2000)

Abstract – The instantaneous velocity field of a circular cylinder wake is built using a PIV technique when a small amount of viscoelastic liquid is introduced through the cylinder. It is shown that the viscoelastic fluid slows down the vorticity concentration and produces a street of partially rolled-up vortices. The underlying mechanism appears very analogous to that of a surface tension in the Kelvin–Helmholtz instability. The partial roll-up is studied in terms of the Weiss determinant. This quantity is a local measurement of the spatial separation between the strain and vorticity. In the viscoelastic wake, the Weiss determinant reaches much lower values than in the Newtonian wake. This result shows that the elasticity prevents the clear separation between vorticity and strain during the roll-up process. Since the Weiss determinant is directly related to the pressure field, it suggests that elasticity can drastically modify the pressure levels even when vorticity and strain levels are unaffected. © 2001 Éditions scientifiques et médicales Elsevier SAS

viscoelasticity / vorticity concentration / stabilisation / pressure / surface tension

1. Introduction

The Kelvin–Helmholtz instability is an essential ingredient in fluid mechanics at moderate and high Reynolds numbers. From an initial state of parallel shear flow this instability can produce an undulation that rolls-up to form vortices. An archetypal flow that reveals such behaviour is the flow around a cylinder. Actually, for sufficiently small Reynolds numbers, the flow is laminar and can be simplified as two shear layers of opposite vorticity in a region localised behind the cylinder. Above a critical Reynolds number, each layer is unstable via a Kelvin–Helmholtz instability, and their coupling produces the periodic Kármán street. There are many studies devoted to the formation of the vortices and to the stability of the street over a wide range of Reynolds numbers (for reviews see Berger and Wille [1], Coutanceau and Defaye [2], Williamson [3]). Recent work (Cadot and Lebey [4], Cadot and Kumar [5], Goldburg [6]) investigates the visualisation of elasticity effects on either the general 2D or 3D spatial structure of a wake. It is shown that elasticity increases the wavelength of the Kármán street (or reduces the Strouhal number as previously observed by James and Acosta [7], Kalashnikov and Kudin [8], Usui et al. [9]) and creates a large region of slow fluid motion behind the cylinder (Delvaux and Crochet [10]). The last effect could also be interpreted as a delay in the roll up process (Cadot and Lebey [4]). These observations appear to be consistent with the stability analysis of a viscoelastic mixing layer due to Azaiez and Homsy [11]. As pointed out by Hinch in appendix E of the same article, elasticity should act as a surface tension in the Kelvin–Helmholtz instability. There are only a few experiments that intend to show the effect of viscoelasticity on 3-D instabilities. In the work of Cadot and Kumar [5], it is shown that the first secondary instability occurring in the wake is mainly damped. They propose a mechanism through which this inhibition could be due to the modification of the basic 2-D flow (flattening of the Kármán vortices.) This idea is supported by the numerical computation of Kumar and Homsy [12].

E-mail address: Olivier.Cadot@univ-lehavre.fr

The aim of the present article is two fold. Firstly, it is to give a quantitative idea of the basic viscoelastic 2-D wake. Secondly, it is to investigate the consequence of this modification on the pressure field. The organisation is the following. We will first briefly recall the experiment. After looking at the results and their analysis, we will discuss the two main issues.

2. The experiment

The apparatus and the injection technique are fully detailed by Cadot and Lebey [4] and Cadot and Kumar [5]. To sum up, the cylinder is pierced with two rows of holes oriented upstream and symmetrically with respect to the main water flow of velocity U. The rate of injection is characterised by the dimensionless ratio: $\beta = u/U$, where u is the mean velocity of the injected liquid at the hole exit. The viscoelastic solution is made from the dilution of PolyEthyleneOxyde at 600 w.p.p.m. in water (see Cadot and Kumar [5] for rheological data.) For the present experiment, the velocity of the flow is $U = 2.8$ cm/s, the cylinder diameter, $d = 5$ mm, the Reynolds number $Re = 140$ (computed from $Re = Ud/\nu$ with ν being the water viscosity). We study three states of injection: no injection at all ($\beta = 0$) corresponding to the unperturbed Newtonian wake; injection of water at $\beta = 0.2$ corresponding to the perturbed Newtonian wake; injection of the viscoelastic solution at $\beta = 0.2$.

For the PIV treatment, only the main flow is seeded with particles. The particle motion, contained in a light sheet of 1 cm in thickness, is then video recorded with a standard digital CCD camera. The portion of the flow on which the PIV treatment is performed is displayed by the dashed rectangle in *figure 1(b)*. We digitalize two consecutive pictures of 728×350 pixels separated by a time duration of 0.16 s. We then compute the intercorrelation between the two pictures using a correlation window of 32×32 pixels. This size fixes the space resolution to $0.8d \times 0.8d$. We obtain a field of displacement vectors over a grid of 22×10. We then interpolate the data over a grid of 440×200 for the computation of velocity space derivatives.

3. Results

Figure 1 shows the visualisation of the wakes for the two states of injection (Newtonian at $\beta = 0.2$ and viscoelastic at $\beta = 0.2$). In the vicoelastic case, the wavelength is increased by a factor 1.4. The formation region behind the cylinder is increased by a factor 3 to 4. Another very striking difference is the large thickening of the braid regions between the vortices. Cadot and Kumar [5] investigated a systematic study of these visualisations varying the Reynolds number, the solution concentration and the injection rate. Here, our attention focuses on the corresponding velocity field displayed in *figure 2* and their analysis.

Figure 2(a) shows the velocity field of the Newtonian wake with no injection at all. The Kármán street is clearly visible. We notice the decrease of the velocity rotation of the vortices as x/d increases due to the viscous diffusion. At smaller distances than $x/d < 10$, we can see the end of the transient region corresponding to the dynamic of the roll up process. For $x/d > 10$ there is a spatial periodic alternative of vortices and saddle points.

We will first examine the periodic region. The vortices are easily repaired as rather circular streamlines and the saddle points as perpendicular cross intersection of streamlines. *Figure 3(a)* shows a sketch of the corresponding streamlines intended to display this topology. The streamlines that pass through the saddle points have tadpole shapes and practically collapse on one another. In the case of the viscoelastic fluid injection, the velocity field presented in *figure 2(c)* display a different wake structure. The Kármán street is still observable and becomes periodic after $13d$. The corresponding sketch of the streamline topology is drawn on *figure 3(b)*; the vortices have now an elliptical shape and the street presents a very large region of streamlines passing between these vortices. This large channel is then responsible in *figure 1(c)* for the large thickness of the braids.

Since the same differences are observed with the Newtonian wake for the same injection parameter β (see *figure 1(b)*), we do conclude that the observed change in the wake structure is due to the viscoelasticity.

During the roll-up process of the Newtonian case ($x/d < 10$), the formed vortices are also elliptic and could also be described by the same streamline topology of *figure 3(b)*. Thus, the roll up process can be viewed as the growth of the tadpole streamlines. A full roll-up would correspond to the collapse of each tadpole on the other (*figure 3(a)*). The streamline topology shows that viscoelasticity somewhat stopped the roll up process.

On *figure 4*, we computed both the square of the vorticity ω^2 and the strain tensor e^2 defined as:

$$\omega^2 = \left(\frac{\partial v_x}{\partial y} - \frac{\partial v_y}{\partial x}\right)^2; \qquad e^2 = 2\left(\frac{\partial v_x}{\partial x}\right)^2 + 2\left(\frac{\partial v_y}{\partial y}\right)^2 + \left(\frac{\partial v_x}{\partial y} + \frac{\partial v_y}{\partial x}\right)^2. \tag{1}$$

(a) Newtonian wake, β = 0.2

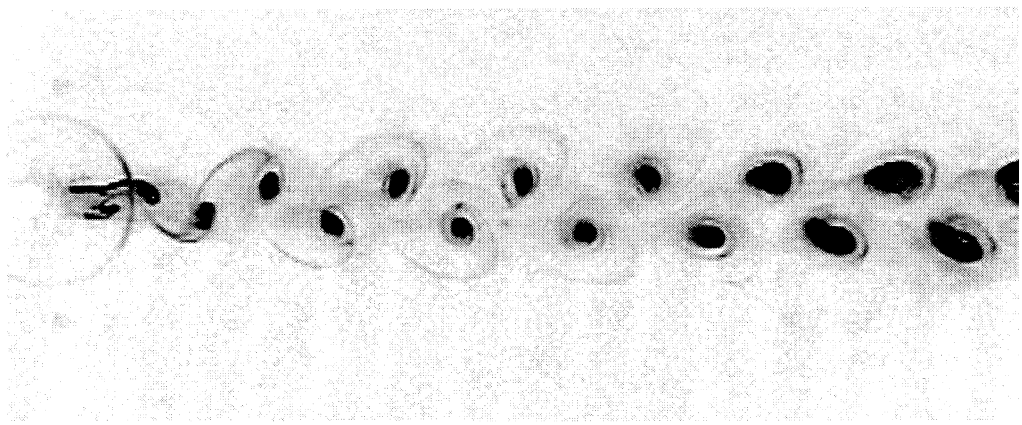

(b) Viscoelastic wake, β = 0.2

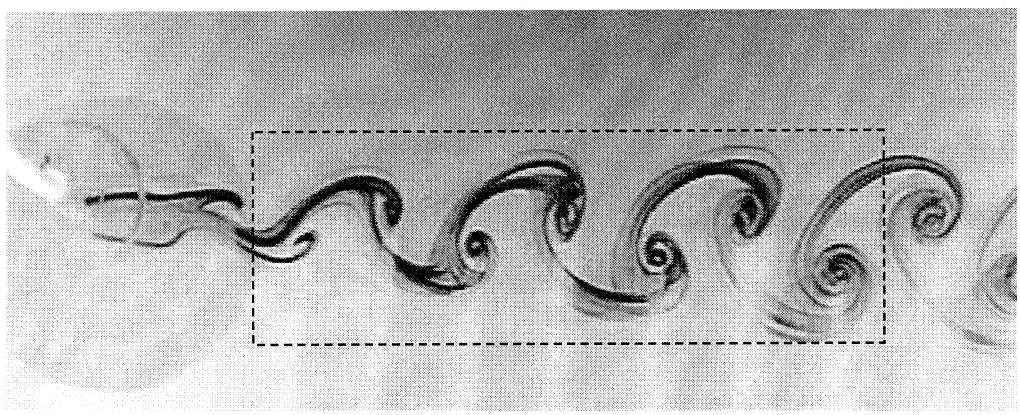

Figure 1. Visualisation of the Kármán street at $Re = 140$ for an injection parameter of $\beta = 0.2$. On picture (a), the injected liquid is simply water while on (b) it is the viscoelastic solution. The dashed rectangle on (b) shows the region of the flow from which further PIV treatment will be done.

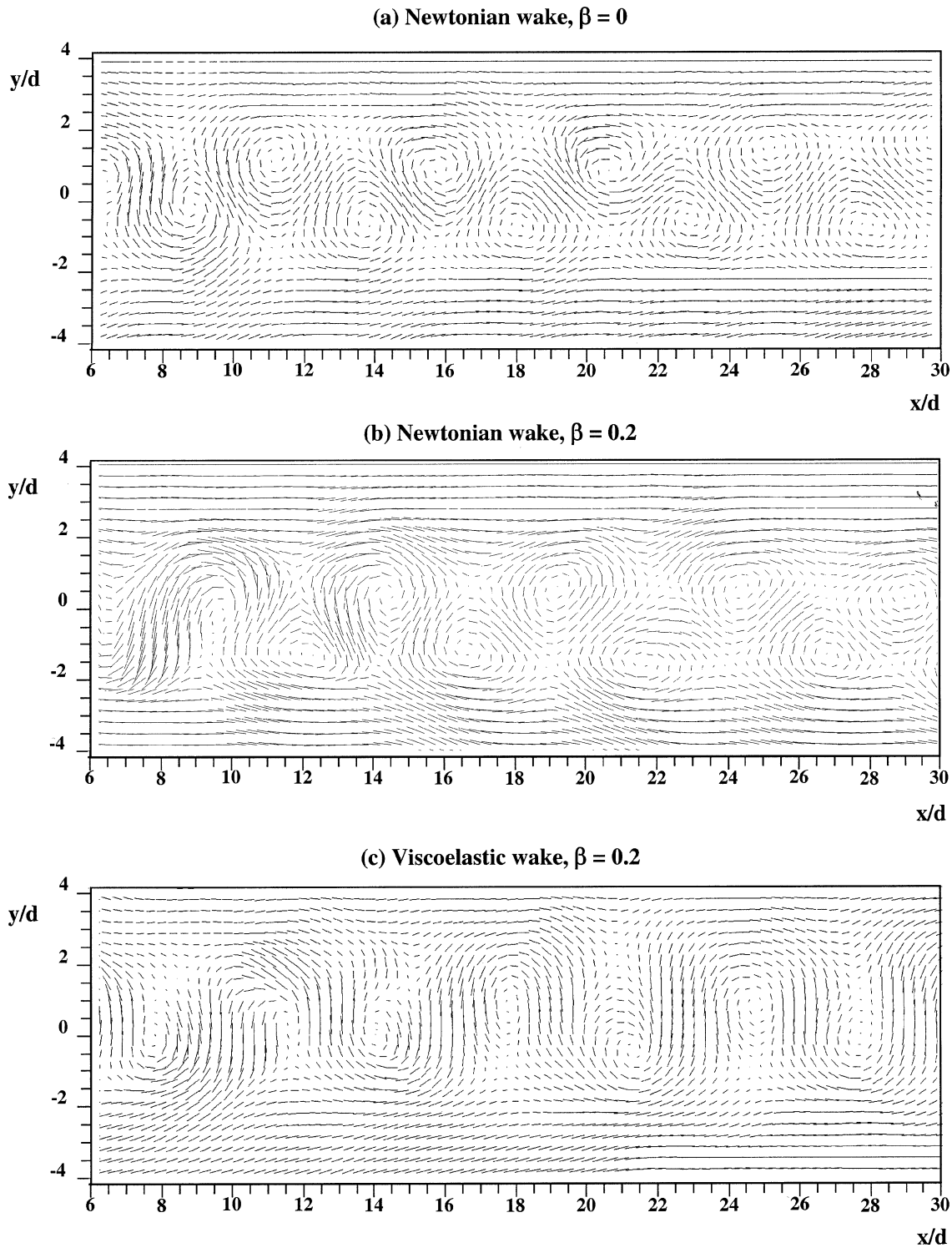

Figure 2. Representation of the velocity field vectors in arbitrary units. The reference frame is the frame where the velocity of the vortices centre is close to 0. $Re = 140$, (a) and (b) corresponds to the Newtonian wakes: (a) with no injection $\beta = 0$; (b) with injection of water at $\beta = 0.2$; (c) corresponds to the injection of the viscoelastic liquid at $\beta = 0.2$.

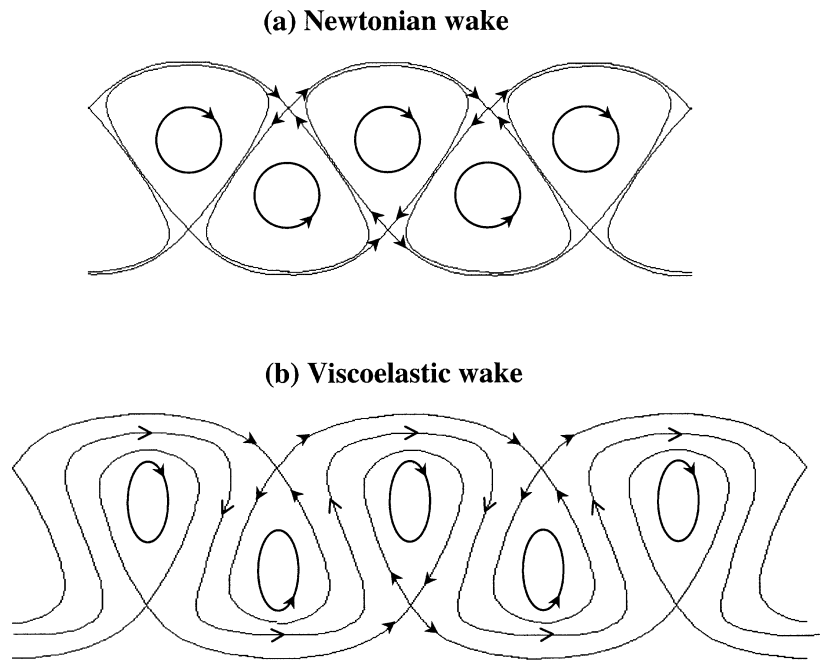

Figure 3. Sketch of the instantaneous streamlines relative to the far wake velocity field obtained in *figure 2* for the case of the Newtonian wakes (a) and the viscoelastic wake (b).

Figure 4 shows the space average in the y and x directions of the vorticity ω^2 (a) and the strain e^2 (b) for the three states of injection. On the left hand side of the figure, each vorticity maximum and strain corresponds to a vortex and saddle point, respectively. During the vortex formation, $x/d < 13$, the values of both the strain and the vorticity are larger for the Newtonian wake, but once the street is periodic, around $x/d > 13$, both quantities remain fairly comparable. The right-hand side of *figure 4* shows the averaging in the x direction. The vorticity and strain distribution clearly present two maxima for the Newtonian wake. The separation between the maxima corresponds to the vertical distance between the two rows of vortices. This separation is not as clear in the case of the viscoelastic wake where strain and vorticity are rather localised in the middle of the wake. A better way to quantify the spatial separation between vorticity and strain is the Weiss determinant defined as:

$$Q(x, y) = \omega^2 - e^2. \tag{2}$$

The map of Q is shown in *figure 5*. Actually, in the Newtonian cases in *figures 5(a)* and *5(b)*, we find that in the far wake, the extrema of Q corresponds to the maxima of ω^2 and e^2 meaning that there is a clear spatial separation between vorticity and strain. This is mostly due to the circular shape of the vortices in the street displayed by the velocity field in either *figure 2(a)* or *2(b)* and by its streamline sketch in *figure 3(a)*. The Q extrema reach lower values in the case of the viscoelastic wake even in the periodic region for $x/d > 13$ where both vorticity and strain are equivalent to the Newtonian case. The reduction of Q is then related to a partial separation of vorticity and strain.

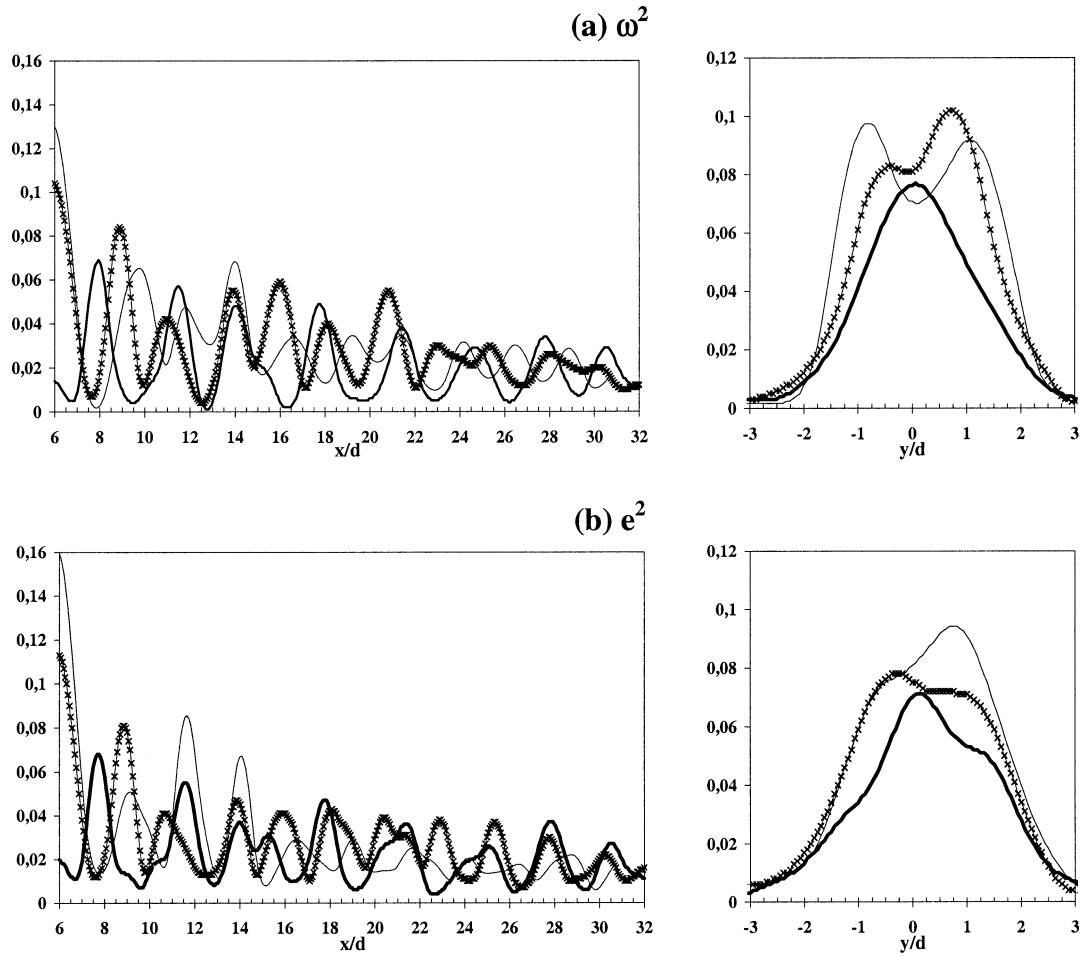

Figure 4. Space average in the y (left) and x (right) direction of the vorticity ω^2 (a) and the strain e^2 (b) obtained from the velocity fields of *figure 2*. The line with crosses corresponds to the Newtonian cases at $\beta = 0$. The thin lines correspond to the Newtonian case at $\beta = 0.2$ and the thick lines refer to the viscoelastic injection at $\beta = 0.2$.

4. Discussions

4.1. Analogy with a surface tension effect

There are several numerical studies due to Pullin [13] and Rangel and Sirignano [14] of the inviscid Kelvin–Hemholtz instability with surface tension between two inmiscible fluids having the same density. With no surface tension, the initial uniform vorticity sheet rolls-up as a spiral and the vorticity is concentrated in the centre of the spiral. It is shown that the surface tension stabilises the shear instability at short wavelength. Also, the vorticity concentration in the vortex core is slowed down and eventually stopped. The extreme last scenario leads to two patches of vorticity symmetrically localised on both sides of the vortex centre. Kumar and Homsy [12] saw this behaviour of higher harmonics generation, in the simulation of a viscoelastic free shear layer. For moderate elasticity, they also observed that the resulting vortices were flattened, having then an elliptical shape. Our experiment generates elliptical vortices with a larger wavelength. At the stage of the vortex formation ($x/d < 10$), the vorticity maxima are smaller in the viscoelastic case (*figure 4*) showing that the roll-

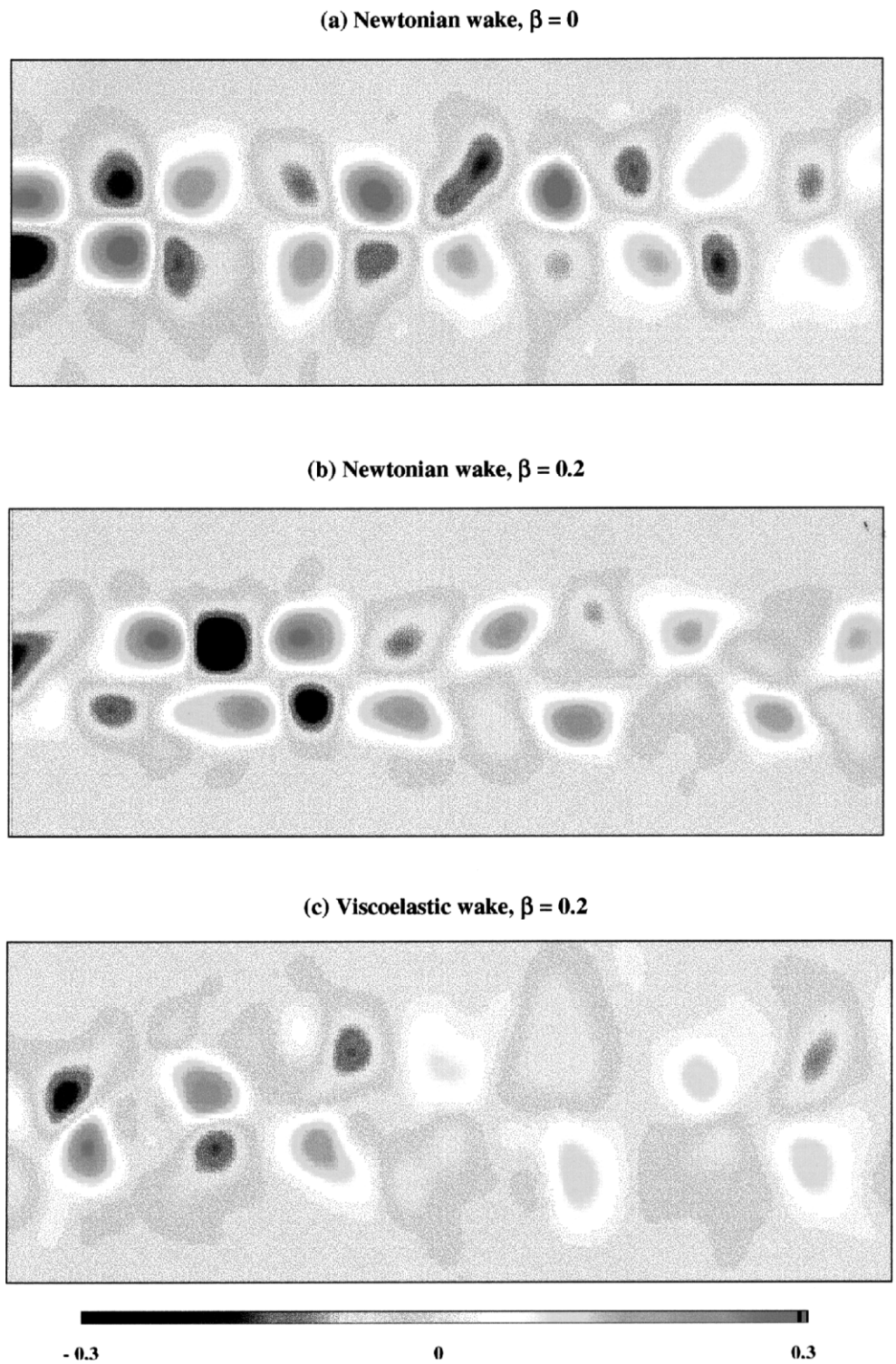

Figure 5. Map of the Weiss determinant $Q = \omega^2 - e^2$ (in arbitrary units) computed from the velocity fields of *figure 2*. The space scales are the same as *figure 2*. (a) is the Newtonian wake $\beta = 0$ (b) is the Newtonian wake $\beta = 0.2$ and (c) is the viscoelastic wake at $\beta = 0.2$.

up is less efficient in concentrating the vorticity into the vortex core. These observations are consistent with a roll-up inhibition and a short wavelength stabilisation of the instability. For $x/d > 10$, the vorticity maxima have the same values as for the Newtonian case, this could be explained by the fact that viscous diffusion relaxes the shear stress downstream the cylinder and then decreases the elastic effects.

4.2. Implications for low pressure structures

In the Navier–Stokes equations Q is proportional to the pressure Laplacian:

$$Q(x, y) = \frac{2}{\rho}\Delta P. \tag{3}$$

Positive or negative extrema of Q correspond to large positive or negative curvatures, respectively of the pressure field and then to local pressure minima or maxima, respectively. The *figure 5(a)* illustrates the pressure distribution for the Newtonian case. When the fluid is viscoelastic, we have to introduce in equation (3) the part of the strain tensor due to elasticity giving:

$$Q(x, y) + \frac{1}{\rho}\vec{\nabla}.\vec{\nabla}\tau = \frac{2}{\rho}\Delta P. \tag{4}$$

The weakening of Q would imply weaker pressure extrema. Also, since the polymer stress gradients are large, one would expect a large effect on the pressure field. This effect could be related to the observation of the reduction of low-pressure structures in a turbulent flow by polymer additives (Bonn et al. [15], Cadot et al. [16]).

5. Conclusion and perspectives

The local injection of a viscoelastic liquid through a cylinder modifies the wake instability and leads to a new type of flow. The formation length is increased and the vorticity concentration is weaker in the transient region close to the cylinder. In the far wake, the periodic street consists of elliptical vortices, separated by thick braid regions. All of these observations are analogous with a scenario of surface tension effect in the Kelvin–Helmholtz instability. Both the weakening of vorticity concentration and the partial roll-up suggest a large effect on the pressure field of the formed vortex.

For a fully turbulent flow, a similar mechanism could be expected when a viscoelastic liquid is injected into the flow. Elasticity could then inhibit the low-pressure region by working against the separation of vorticity and strain. If such a mechanism occurs in turbulent flows of drag reducing solutions, will it only affect the low pressure structures formation, or will it also influence the measured drag?

Acknowledgements

The author would like to thanks Elie Rivoalen and Satish Kumar for the very fruitful discussions and helpful remarks.

References

[1] Berger E., Wille R., Periodic flow phenomena, Ann. Rev. Fluid. Mech. 4 (1972) 313.

[2] Coutanceau M., Defaye J.-R., Circular wake configurations; a flow visualization survey, Appl. Mech. Rev. 44 (6) (1991) 255–305.
[3] Williamson C.H.K., Vortex dynamics in the cylinder wake, Ann. Rev. Fluid. Mech. 28 (1996) 447–540.
[4] Cadot O., Lebey M., Shear instability inhibition in a cylinder wake by local injection of a viscoelastic fluid, Phys. Fluids 11 (1999) 494–496.
[5] Cadot O., Kumar S., Experimental characterization of viscoelastic effects on two- and three-dimensional shear instabilities, J. Fluid. Mech. 416 (2000) 151–172.
[6] Goldburg W.I., Private communication, 1999.
[7] James D.F, Acosta A.J, The laminar flow of dilute polymer solutions around circular cylinders, J. Fluid Mech. 42 (1970) 269–288.
[8] Kalashnikov V.N., Kudin A.M., Kármán vortices in the flow of drag-reducing polymer solutions, Nature 225 (1970) 445.
[9] Usui H., Shibata T., Sano Y., Kármán vortex behind a circular cylinder in dilute polymer solutions, Chem. Eng. J. Japan 13 (1) (1980) 77–79.
[10] Delvaux, V., Crochet M.J., Numerical prediction of anomalous transport properties in viscoelastic flow, J. Non-Newtonian Fluid Mech. 37 (1990) 297–315.
[11] Azaiez J., Homsy G.M., Linear stability of free shear flow of viscoelastic liquids, J. Fluid Mech. 268 (1994) 37–69.
[12] Kumar S., Homsy G.M., Direct numerical simulation of hydrodynamic instabilities in two- and three-dimensional viscoelastic free shear layer, J. Non-Newtonian Fluid Mech. 83 (1999) 249–276.
[13] Pullin D.I., Numerical studies of surface tension effects in nonlinear Kelvin–Helmholtz and Rayleigh–Taylor instability, J. Fluid Mech. 119 (1982).
[14] Rangel R., Sirignano W., Nonlinear growth of the Kelvin–Helmholtz instability; Effect of surface tension and density ratio, Phys. Fluids 31 (1988) 1845.
[15] Bonn D., Couder Y., van Dam P.H.J., Douady S., From small scales to large scales in three dimensionnal turbulence: the effect of diluted polymers, Phys. Rev. E 47 (1) (1993) R28–R31.
[16] Cadot O., Bonn D., Douady S., Turbulent drag reduction in a closed flow system: boundary layer vs. bulk effect, Phys. of Fluids 10 (2) (1998) 426–436.